Static and Dynamic Studies on LiNi$_{1/3}$Co$_{1/3}$Mn$_{1/3}$O$_2$-Based Suspensions for Semi-Solid Flow Batteries

Jordi Jacas Biendicho,*[a] Cristina Flox,[a] Laura Sanz,[a] and Joan Ramon Morante[a, b]

LiNi$_{1/3}$Co$_{1/3}$Mn$_{1/3}$O$_2$ (LNCM)-based suspensions for semi-solid flow batteries (SSFB) have been investigated by galvanostatic charge/discharge an electrochemical impedance spectroscopy (EIS). The resistance and electrochemical performance of half cells (vs. Li/Li$^+$) as well as the rheological properties are affected by the content of a commercially available electroconductive carbon black [KetjenBlack (KB), AkzoNobel] in the suspensions. In static conditions, a cell with 11.87 and 13.97 % by volume of KB and LNCM delivers high capacity 130 mAh g^{-1} at 5 mA cm^{-2}, respectively, and a coulombic efficiency of 90 % over 10 injections. The impedance of half cells is dominated by a contact resistance fitted with a resistor and a constant phase element (CPE) in parallel. In flow conditions, cell potential depends on applied current density and measured over potentials are ~0.3 and 0.7 V for 0.33 and 1 mA cm^{-2}, respectively, for a cell containing a suspension with 9.53 % in volume of KB and 13.90 % in volume of LNCM. The effect of the cell contact resistance on the electrochemical performance is discussed.

Introduction

A flow battery is an energy system in which at least one of the electrolytes is pumped between the electrolyte tank and the electrochemical cell. From the original redox flow battery (RFB) developed in the late 1970s,[1] other flowable systems have been investigated and their chemistry reviewed in Refs. [2] and [3]. In this frame, the all-vanadium redox battery (VRB)[4–6] is the most promising energy-storage system, well-suited for medium and large scale applications to store intermittent renewable energy. However, it suffers from low specific energy owing to the limited solubility of vanadium species and the narrow potential window of operation of these aqueous electrolytes. In this scenario, Chiang and co-workers[7] reported a new energy-storage system or semi-solid flow battery (SSFB) that would amend these issues and simultaneously preserve the typical advantages of a RFB: flexibility in configuration and operation, as well as energy and power decoupling. Figure 1 shows a sketch of a SSFB. Positive and negative suspensions contain lithium intercalation compounds and conductive parti-
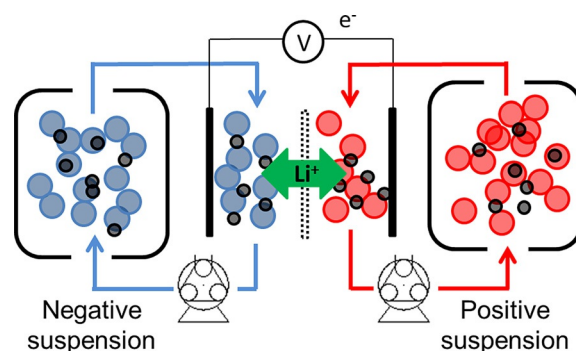
Figure 1. Sketch of a SSFB in which lithium intercalation compound and conductive additive are presented as colored and black spheres, respectively, for the positive and negative suspensions.

cles both in suspension. To release the chemical energy of a SSFB, suspensions are pumped into the electrochemical cell where the reaction takes place, while the electrons are transferred to the current collector closing the external electrical circuit. The use of organic solvents combined with lithium-intercalation compounds maximizes energy density. For instance, a suspension containing ~25 % in weight of LiNi$_{1/3}$Co$_{1/3}$Mn$_{1/3}$O$_2$ (LNCM) could potentially have an energy density of 252 Wh kg^{-1} and this is an order of magnitude higher than the energy density of a VRB that is, 20–30 Wh kg^{-1}, in which the concentration of vanadium species is around 2.0 M in acidic aqueous electrolytes.[4–6] All these perspectives make SSFBs a very promising energy system with many potential applications even in the automotive industry.

From the materials point of view, we can take advantage of the extensive work conducted on intercalation compounds for Li-ion batteries in terms of composition, structure, properties, and use materials that are able to store large amounts of energy. In this sense, suspensions of Li$_4$Ti$_5$O$_{12}$ (LTO),[8,9] Si,[10] or LiCoO$_2$[7] have been recently characterized as negative and pos-

[a] Dr. J. J. Biendicho, Dr. C. Flox, Dr. L. Sanz, Prof. J. R. Morante
    Catalonia Institute for Energy Research
    Jardins de les Dones de Negre 1, 08930 Sant Adrià del Besos (Spain)
    E-mail: jjacas@irec.cat

[b] Prof. J. R. Morante
    Departament d'Electronica
    Universitat de Barcelona
    C. de Martí I Franquès 1, 08028 Barcelona (Spain)

Supporting Information and the ORCID identification number(s) for the author(s) of this article can be found under http://dx.doi.org/10.1002/cssc.201600285.

itive suspensions, respectively. On the other hand, carbon black is the most common additive used to improve the conductivity of the composites for Li-ion batteries, as it forms a percolating conductive network that ensures an effective electron transfer between the electroactive particles and the current collectors. The role of carbon black on the electrochemical and rheological properties of suspensions has been investigated by several authors.[11–13] It appears that the amount of carbon black necessary to form a conductive network depends on several factors ranging from the preparation method to the wt% of electroactive particles in the suspensions. In this sense, suspensions with various wt% of LTO and prepared by the ball-milling method were characterized as a function of channel thickness in static conditions;[9] however, their stability over time has recently been discussed.[14] Little characterization has been done on the factors that hinder or promote the electrochemical performance of semi solid suspensions in flow conditions.[8, 13, 15]

EIS is a valuable technique that can be used to identify the factors that limit the performance of the electrodes in an energy-storage system. In this sense, relevant work has been done on the field of Li-ion batteries in which the various impedance contributions have been discussed and equivalent circuit models extracted using fitting.[16–19] These impedance contributions commonly show a non-ideal behavior, which can be identified, for instance, by a depressed semicircle in the Z' versus Z'' plot. An element that is commonly included to enable equivalent circuits to fit non-ideal experimental data is the constant phase element (CPE), whose admittance is defined as: $Y^* = Q(j\omega)^n$, where $j = \sqrt{-1}$, $\omega = 2\pi f$, f is the measuring frequency, and n is a power law exponent with value in the range $0 < n < 1$. If $n = 0$, Y^* behaves as a pure resistor, and if $n = 1$, Y^* behaves as a pure capacitor, taking Q values of $1/R$ and C, respectively.

In this paper, we present a detailed study of LNCM-based suspensions for SSFBs in both static and dynamic conditions. We have selected LNCM because it is a material that can store a large amount of energy with improved structural stability and lower cost compared to the pristine $LiCoO_2$.[20,21] Suspensions have been prepared by magnetic stirring and the volume percentage of a commercially available electroconductive carbon black [KetjenBlack (KB), AkzoNobel] tuned to evaluate the effect of the conductive additive on the electrical and electrochemical properties of suspensions measured by EIS and charge/discharge experiments, respectively, in both static and flow conditions. Results are of interest to improve formulation as well as fundamental understanding of the factors that limit the electrochemical performance of semi-solid suspensions.

Results and Discussion

The X-ray diffraction pattern (XRD) and scanning electron microscope (SEM) picture of LNCM are presented in Figure 2a and b, respectively. Diffraction peaks are sharp indicating high crystallinity of the sample and are indexed using a romhohedral unit cell with lattice parameter $a = 2.86$ (1) and $c = 14.19$ (1) Å with $V = 100.52$ (1) Å^3 in agreement with reported phases with
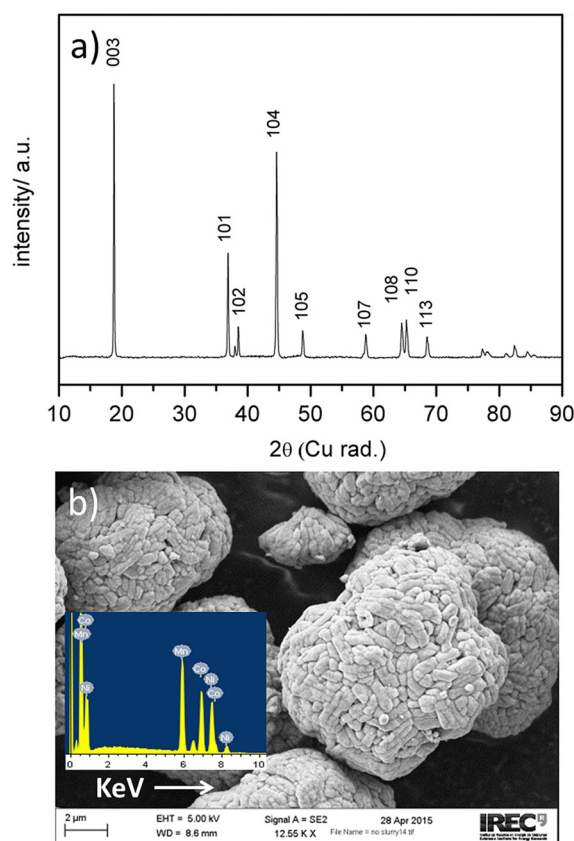
Figure 2. a) XRD pattern and b) SEM picture and EDX analysis of LNCM powder as received from Toda America©.

similar composition.[22] The SEM picture shows LNCM particles aggregate forming clusters of 8–10 μm, and their average atomic ratio is 33.75, 33.51, and 32.72% for Mn, Co, and Ni, respectively.

Suspensions prepared in this manuscript are shown in Table 1 in the form of vol%, volumetric capacity, and grams of KB and LNCM. The vol% of KB was varied, whereas the volume of solvent [i.e., 1 M $LiPF_6$ in 1:1 w/w ethylene carbonate (EC)/dimethyl carbonate (DMC)] was fixed to 6 mL. In this way, we were able to monitor the effect of KB on suspensions containing LNCM as the intercalation compound. Small volumes of suspensions were deposited on SEM holders and dried overnight inside the glove box. Figure 1 in the Supporting Information shows a SEM picture of a dried suspension. LNCM particles

Table 1. Composition of prepared suspensions.[a]

Suspension	KB [vol%]	LNCM [vol%]	Capacity [AhL^{-1}]	KB [g]	LNCM [g]
1	1.70	13.45	47.11	0.03	2.38
2	3.85	13.61	47.57	0.07	2.47
3	7.95	13.82	48.27	0.15	2.64
4	9.53	13.90	48.52	0.19	2.72
5	11.87	13.97	48.81	0.24	2.82

[a] LNCM as the intercalation compound, KB is carbon black, and 1 M $LiPF_6$ in 1:1 EC/DMC as the electrolyte; capacity calculations are limited to $x = 0.5$ in L_xNCM.

remain aggregated after magnetic stirring and are surrounded by KB. The picture resembles a conglomerate owing to the spherical shape of the LNCM clusters.

Half cells containing the suspensions listed in Table 1 were characterized by EIS. Representative Z' versus Z'' plots of discharged cells in dynamic mode that is, suspensions constantly flowing between tanks and cells, are presented in Figure 3a.
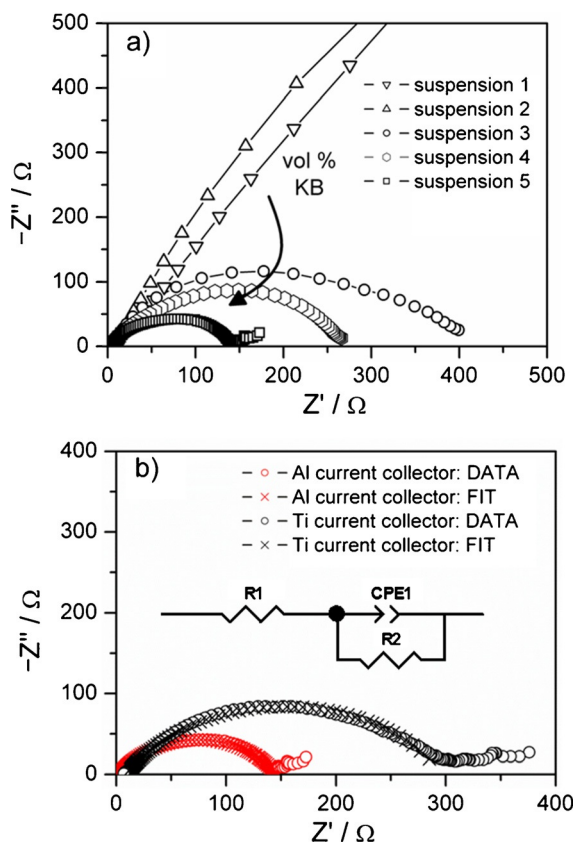
Figure 3. a) Z' versus Z'' plots of half cells containing suspensions with different vol % of KB. b) Fits to impedance data using model inset for a half cell with suspension 5. Red and black traces correspond to data collected using Al and Ti current collectors, respectively.

A single Z' intercept is observed for cells containing suspensions 1 and 2, hence with low vol % of KB. For half cells containing suspensions with high vol % of KB, suspensions 3, 4, and 5, two Z' intercepts are observed at high and low frequency. Table 2 shows resistance (Ω) and area-specific resistance ($\Omega\,cm^2$) values for the cells. The high frequency intercept is attributed to electrolyte resistance, as well as other "ohmic" contributions, as its magnitude [i.e., 7 mS cm^{-1} (the geometrical factor of the cell is 29.6 cm)] does not vary as a function of the content of KB and, in addition, this conductivity is on the same order of magnitude as the conductivity reported for non-aqueous electrolytes with similar composition (e.g., 1–10 mS cm^{-1}).[23] On the other hand, the low frequency Z' intercept becomes less resistive as the volume of KB increases in the suspension. At certain vol % of KB (i.e., ≥ 7.95), an impedance semicircle is formed. In fact, Z' versus Z'' plots for half cells with suspensions 3, 4, and 5 are very similar to impedance

Table 2. Resistance (R) and area specific resistance (ASR) values of half cells (vs. Li/Li$^+$) as obtained from the high and low frequency Z' intercepts in Z' versus Z'' plots.

Suspension	High frequency Z' intercept		Low frequency Z' intercept	
	R [Ω]	ASR [$\Omega\,cm^2$]	R [Ω]	ASR [$\Omega\,cm^2$]
1	5.7	16.8	26 902	79 630
2	6	17.7	6396	18 932
3	4.4	13	405	1199
4	3.5	10.4	270	800
5	3.4	10	140	414

plots measured for discharged Li-ion batteries.[18–21] Impedance semicircles in Figure 3a are clearly non-ideal and a CPE[24] instead of a capacitor is necessary to fit the impedance data. Figure 3b shows the impedance fit using a parallel combination of a resistor and a CPE for a cell containing suspension 5. Visual inspection of the fit shows good agreement between the model and experimental data, presented as circles and crosses, respectively.

Capacitance values for the fitted semicircles are 12 and 4 $\mu F\,cm^{-2}$ for suspensions 3 and 5, respectively. This magnitude of capacitance (μF) indicates that the semicircle in the Z' versus Z'' plots is related to an interface response[25] or contact resistance between the current collector and the suspension, an impedance contribution commonly observed on ceramic pellets[26, 27] as well as in Li-ion batteries.[18] To gain information of the factors governing the impedance of this semicircle, we assembled a half cell using suspension 5, but replacing aluminum by titanium as current collector. Impedance data and the fit using the equivalent model previously described are presented in Figure 3b. The impedance of the semicircle increases from 150 to 300 Ω; however, the fitted capacitance remains unaffected $\sim 4\,\mu F\,cm^{-2}$. This confirms that the impedance semicircle observed in Z' versus Z'' plots is related to a contact resistance in agreement with previous impedance studies on SSFB as a function of grain size used to polish the current collectors.[9]

At low frequency, a very poorly resolved inclined spike is observed in Z' versus Z'' plots (Figure 3b) and, unfortunately, we were unable to fit data in this frequency range even though a second CPE was added in series. Nevertheless, the associated capacitance of the spike, calculated from the relation $C = 1/\omega Z''$, is on the order of approximately 200 mF cm^{-2} and has been attributed to the double layer capacitance of KB particles in suspension as measured by cyclic voltammetry.[9]

Electrochemical performance of half cells

In the following section, the electrochemical performance of half cells with suspensions listed in Table 1 are evaluated in both static- and dynamic-flow conditions.

Static mode

The electrochemical performance of suspensions 1 and 2 are very poor, even at current densities as low as 0.1 mA cm^{-2}

(data not shown). This is expected owing to the high resistance of both cells listed in Table 2. The cell with suspension 3, however, delivers 125 and 131 mA h g^{-1} at 0.25 and 0.50 mA cm^{-2} on discharge, respectively. Voltage profiles versus time are shown in Figure 2 in the Supporting Information. The cell shows significant over potentials compared to a porous LNCM electrode[28] so higher current densities (i.e., >0.50 mA cm^{-2}) were not attempted. On the other hand, the cell with suspension 5 shows much better electrochemical performance as shown in Figure 4a and b. Rate capability tests
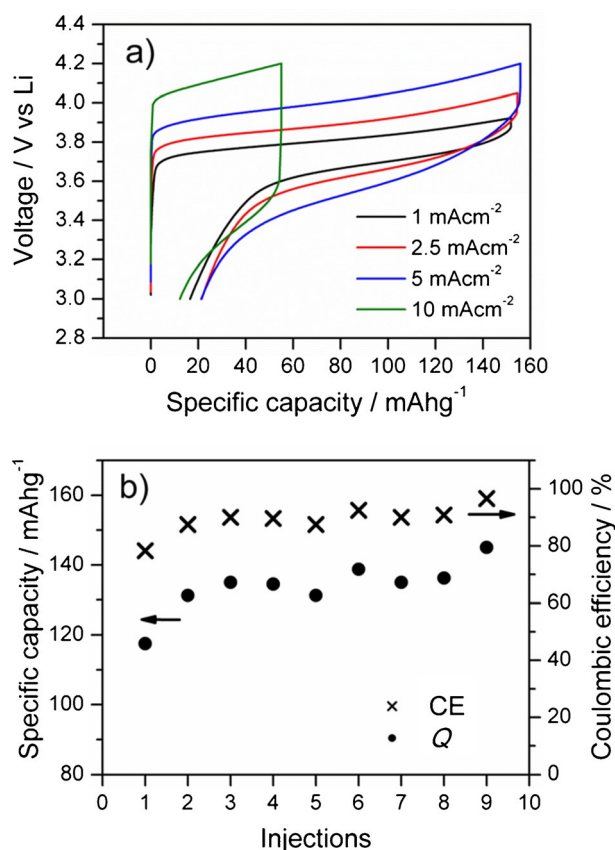
Figure 4. a) Voltage versus specific capacity profiles of a half cell with suspension 5. Several current rates were applied: 1, 2.5, 5, and 10 mA cm^{-2}. b) Specific discharge capacity and coulombic efficiency of the cell over several injections. A current of 2.5 mA cm^{-2} was applied.

(i.e., voltage versus capacity at different current rates; Figure 4a) indicate that the cell delivers 135, 128, and 127 mA h g^{-1} at 1, 2.5, and 5 mA cm^{-2}, respectively. The cell capacity, however, reduces to 41 mA h g^{-1} at 10 mA cm^{-2}. Assuming a total capacity of 150 mA h g^{-1}, current densities correspond to C/5, C/2, 1C, and 2C, respectively, and ~85% of the stored charge is delivered at high current rates (i.e., C/2 or 1C). Voltage versus specific capacity profiles in Figure 4a resemble a porous electrode with minimum over potentials at significant current rates. Complementary to these analyses, electrochemical data in intermittent mode is presented in Figure 4b in the form of Q and coulombic efficiency (CE). In intermittent mode, the channel of the electrochemical cell is filled with fresh sus-

pension pumped from the reservoir tanks after each charge/discharge cycle. An average discharge capacity of 130 mA h g^{-1} and a CE of 90% at C/2 are obtained over 10 injections.

Therefore, it is crucial to add a certain amount of KB in the suspensions to extract the maximum charge stored within the LNCM particles. If a low vol% of KB is used (e.g., suspensions 1 and 2) the conductive network is not formed and LNCM particles remain isolated and not wired to current collector leading to a very poor electrochemical performance as it was anticipated by the large resistance of cells extracted from EIS analysis. As the vol% of KB increases (e.g., suspension 3), significant amounts of charge are extracted from the cell, but at low current densities. Electrons are able to reach the current collector, but over potentials (Figure 2 in the Supporting Information) and cell resistance (Figure 3a) indicate that the conductive KB network is not completed. Suspension 5 shows the best performance in terms of electrochemistry compared with the rest of the cells. The structure of the carbon network is much improved in this suspension and the battery delivers large capacities at higher current rates, implying that the majority of the LNCM particles are connected to the current collector. Results demonstrate that the main kinetic limitation of LNCM-based suspensions is not related to Li-ion transfer but to electronic conduction, even though the conductivity of LNCM is relatively high and predominantly electronic (~10^{-4} S cm^{-1})[29] when compared with other Li-intercalation compounds (~10^{-9} S cm^{-1} for bare LTO).[30]

Flow mode

To effectively decouple the energy and power densities, and maximize the battery capacity of traditional Li-ion systems, the SSFB should be able to operate in dynamic mode, in which suspensions (both positive and negative) stored in tanks are constantly recirculated through the electrochemical cell. Previously, to perform the electrochemical measurements in dynamic conditions, the viscosity of the different suspensions listed in Table 1 was investigated to ensure an appropriate flowability of the mixture during the operation of the battery. All the suspensions measured presented a shear-tinning behavior when the shear rate was varied, indicating a pseudo plastic behavior as can be observed in Figure 5. Viscosity of suspensions 1–3 are between 10 to <1000 cP depending on the KB content. These viscosities are in the same order of magnitude as those measured for LTO-based suspensions with 2 wt% of KB.[31] Suspension 5 is, as expected, more viscous than suspensions 1–3 owing to the higher content of KB (i.e., 2.2 wt% of KB). Its viscosity shows two shear-thinning regions at low and high shear rates separated by a shear-thickening (or plateau) region over intermediate shear rates that has been previously reported and explained for concentrated suspensions.[12]

To enhance hydrodynamics, while maintaining good electrochemical performance of the suspension, we decided to test suspension 4 {i.e., 9.53 and 13.90 vol% of KB and LNCM, respectively. The viscosity of suspension 4 is lower than suspension 5 (i.e., <1000 cP at shear rates >10 s^{-1}) and also shows the shear-thickening in the region 1–10 s^{-1}, indicative of the

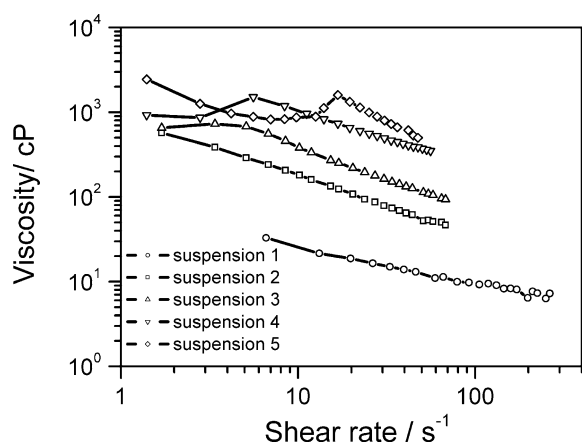**Figure 5.** Viscosity values as a function of shear rate for suspensions 1–5.
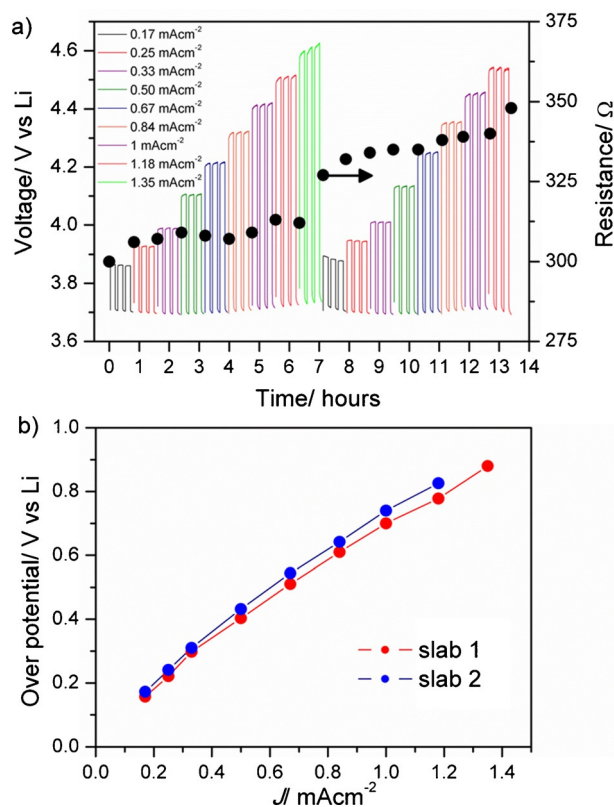

Figure 6. a) Voltage versus time profiles and impedance of the half cell with suspension 4 operating in flow mode. Positive charge pulses at different current densities were intercalated between open circuit voltage periods and impedance measurements. Applied current densities are color coded. b) Measured cell over potential as a function of current density on charge. Red and orange traces correspond to two time slabs.

breakup of the KB network, which is accompanied by a steep drop in suspension conductivity.[14] Suspension 4 was selected to conduct electrochemical measurements in flow conditions owing to its improved rheological properties compared to suspension 5, while preserving the percolation network of KB.

Figure 6a shows voltage profiles, as well as the cell impedance versus time measured in flow mode for suspension 4. The suspension was pumped between the reservoir tanks and the electrochemical cell using a flow rate of 2 mL min^{-1}. First, the cell was charged at 0.33 mA cm^{-2} overnight to reach the characteristic LNCM charge plateau as previously observed in static measurements (i.e., ~3.7 V) and then short pulses of charge, open-circuit voltage periods, and impedance measurements were intercalated. Applied current densities were 0.17, 0.25, 0.33, 0.50, 0.67, 0.84, 1, 1.18, and 1.35 mA cm^{-2}, and resistance values were obtained from impedance semicircles with associated capacitance values in the range of 2–6 µF cm^{-2} associated with the interface between the current collector and the suspension. By conducting this type of experiment, we measured the cell over potential as a function of current density, as shown in Figure 6b.

Measured over potentials are ~0.3 and 0.7 V for 0.33 and 1 mA cm^{-2}, respectively. The cell potential quickly increases to a value proportional to the iR drop, where i refers to applied current and R to cell resistance; therefore, the relationship between the voltage and current is linear and the slope of this linear curve depends on the resistance. In addition, small but significant variations in the cell contact resistance are observed versus time and match relaxation periods after a peak in current density. This indicates a certain degree of polarization within the electrochemical cell which, most likely, is related to the re-organization of the KB particles at the interface between the suspension and the current collector. The effect of the channel size dimension and suspension flow rate on the cell over potentials were also evaluated; Figure 3a and b in the Supporting Information, respectively. Over potentials increase when the channel width increases from 4 to 8 mm (i.e., 0.7 and 0.94 V at 1 mA cm^{-2}, respectively). However, they are independent of the suspension flow rate (e.g., 0.94 and 0.92 V for 2 and 5.6 mL min^{-1} measured at 1 mA cm^{-2}, respectively).

The cell with suspension 4 (Figure 6) was charged for longer times, but its electrochemical performance was not reproducible after 13 h of operation in flow mode. Figure 4a and b in the Supporting Information show the cell resistance and over potentials as a function of time, respectively. After 13 h, the cell contact resistance decreases abruptly to 175 Ω and, in turn, leads to lower cell over potentials (blue trace in Figure 4b in the Supporting Information). The contact resistance, however, reverts to a value of ~350 Ω after adding solvent to the suspension tank, as shown by the red arrow in Figure 4a in the Supporting Information. The viscosity and electro-rheological properties of semi-solid suspensions change as a function of shearing (analogous to flowing conditions)[12, 32] and their stability over time has been recently discussed and improved by adding a surfactant to the mixture. However, the manuscript only showed measurements in static conditions.[14] In this sense, we are currently working on the optimization of the cell components and evaluating other preparation methods for example, ball-milling, as well as testing potential additives to achieve reliable SSFBs with good efficiency operating in dynamic flow mode.

Conclusions

The effect of a commercially available electroconductive carbon black [KetjenBlack (KB), AkzoNobel] on $LiNi_{1/3}Co_{1/3}Mn_{1/3}O_2$ (LNCM)-based suspensions prepared by magnetic stirring has been investigated by assembling half cells (vs. Li/Li^+) in both static and dynamic flow conditions.

In static conditions, the electrical and electrochemical performance of cells containing suspensions with low vol% of KB is poor owing to their large resistance (i.e. $>5000\ \Omega$). As the vol% of KB increases (i.e., $\geq 8\%$), cells deliver large capacities discharged at fast current densities when the KB network is completed, implying that nearly all LNCM particles are connected to the current collector (i.e., $130\ mA\,h\,g^{-1}$ at $5\ mA\,cm^{-2}$ for a suspension with 11.87% in volume of KB).

In flow mode, we have monitored the voltage as a function of current density as well as the cell impedance for a suspension with 9.53 vol% of KB and 13.90 vol% of LNCM. Measured over potentials are ~ 0.3 and $0.7\ V$ for 0.33 and $1\ mA\,cm^{-2}$, respectively, and are independent of the suspension flow rate (i.e., 2 and $5.6\ mL\,min^{-1}$). The cell experiences a certain degree of polarization as measured by electrochemical impedance spectroscopy (EIS).

Typical Z' versus Z'' plots of the cells show an impedance semicircle that is fitted by a parallel combination of a resistor and a constant phase element (CPE). Its associated resistance depends on the vol% of KB in the suspensions as well as the type of current collector used to assemble the cell (e.g., Al or Ti). However, its associated capacitance remains in the range of $\sim 4\ \mu F\,cm^{-2}$. From the above, the impedance semicircle is attributed to the interface between the current collector and the LNCM-based suspension. This contact resistance can be tuned, and to some extent controlled, by the use of different materials to construct the electrochemical cell as well as the composition of the semi-solid suspensions. It is of paramount importance to minimize the magnitude of the contact resistance in the semi-solid electrochemical cells and, in turn, improve their electrochemical performance in all operation modes (i.e., static, intermittent, or flow mode).

Experimental Section

Suspension preparation

Suspensions investigated in this manuscript were prepared as follows; LNCM with tap density $2.5\ g\,cm^{-3}$ purchased from Toda America© was mixed with highly conductive Ketjenblack© EC-600 with a tap density of $0.25\ g\,cm^{-3}$ obtained from AkzoNobel and a liquid electrolyte formed with $1\ M\ LiPF_6$ in EC and DMC mixed in the weight ratio 1:1 as obtained from Solvionic©. Various stoichiometries were prepared and mixed using a magnetic stirrer at 1000 rpm for 1 h. The volume of KB in slurries was varied between ~ 2 to 12%. The volume of solvent used to prepare suspensions was fixed to 6 mL. For the suspension with 9.53 vol% of KB investigated in flow mode, the volume of solvent used was 10 mL. It must be remarked that suspensions containing concentrations of KB higher than 11.87 vol% were also prepared, but were no longer liquid enough to be able to flow readily, so they were not considered further. During battery flow mode operation, suspensions were constantly stirred to maintain homogeneity.

Electrochemical cell configuration and components

The electrochemical cell for measuring suspensions has been used previously.[8, 15] The cell consists of several parts that are stacked on top of each other to build either a half cell or a full cell. Two thick teflon pieces act as a frame and give strength to the battery. A copper plate was used as current collector for the counter electrode or Li metal and Al and Ti plates were used as positive suspension. Metallic plates were polished prior to cell assembly using 1000 grit sandpaper. The cell channel was defined by two types of teflon pieces: hard and expanded, with dimensions of $74\times 4\times 1\ mm$ (length$\times$width$\times$thickness). A polypropylene membrane Celgard 2500 was used to separate positive suspension and Li metal. In order to pump the LNCM based suspensions into the electrochemical cell, a digital peristaltic pump from Major Science© model Mu-D02 was used in combination with Materflex© tubing.

Electrochemical characterization

Assembly and characterization of flow batteries was conducted in an Ar-filled glove box ($O_2 < 1$ ppm and $H_2O < 1$ ppm) and electrochemical properties investigated both in static, intermittent and flow mode using a Bio-Logic VSP300 potentiostat with an EIS expansion set. EIS data were collected in galvanostatic control mode or GEIS[33] using EC-lab[34] in the frequency range 200 KHz to 100 mHz and transformed to Zview[35] format to plot and fit impedance data, as necessary.

The energy contained in SSFBs can be extracted using different operational modes (i.e., (static, intermittent, and flow mode). Static mode corresponds to loading the channel of the cell with the suspension and conducting electrochemical characterization, similar to a porous Li-ion electrode material. The intermittent mode refers to replacing the suspension contained in the channel by a fresh one from the reservoir tank after a charge/discharge cycle. And the flow mode involves suspension to be constantly flowing between the tanks and the electrochemical cell. For the last, flow rates of 2 and $5.6\ mL\,min^{-1}$ were used.

Layered rock-salt electrode materials, such as LNCM, undergo significant structural changes as a function of state-of-charge (SOC). For instance, $LiCoO_2$ transforms to a monoclinic phase when $x \approx 0.5$ in $Li_{1-x}CoO_2$[16,17] and, in turn, the electrode suffers sever capacity fading on cycling. In the monoclinic phase, lithium intercalation is not reversible. Therefore, the cell capacity was limited to $150\ mA\,h\,g^{-1}$ or $x = 0.55$ in the formula $Li_{1-x}Ni_{1/3}Co_{1/3}Mn_{1/3}O_2$ for measurements conducted in static and intermittent mode. In addition, an upper cut-off voltage of 4.2 V was used. For data collected in dynamic mode, the upper cut-off voltage was increased to 4.6 V.

Viscosity measurements

The viscosity of the samples was measured using a rotational viscometer DV2T Brookfield in a range of shear rates corresponding to rotational speeds from 5 to 200 rpm. Different spindle sizes (SC-18, SC-31, and SC-34) were used to handle the more and the less viscous suspensions, in accordance with the viscosity ranges of the different samples. Measurements were repeated three times to check reproducibility.

Structural and particle morphology characterization

Structural information of the LNCM powder was obtained by XRD using a Bruker AXS D8 ADVANCE X-ray diffractometer with $CuK_{\alpha1}$ radiation in the 2θ range 10–100° using 0.1° step size. A SEM ZEISS Auriga microscope equipped with an energy dispersive X-ray (EDX) detector with INCA software was used to investigate particle morphology of suspensions as well as their chemical composition.

Acknowledgements

[1] L. H. Thaller, Technical paper NASA TM X-71540, **1974**.
[2] A. Z. Weber, M. M. Mench, J. P. Meyers, P. N. Ross, J. T. Gostick, Q. Liu, *J. Appl. Electrochem.* **2011**, *41*, 1137–1164.
[3] Q. Huang, Q. Wang, *ChemPlusChem* **2015**, *80*, 312–322.
[4] E. Sum, M. Skyllas-Kazacos, *J. Power Sources* **1985**, *15*, 179–190.
[5] C. Flox, C. Fabrega, T. Andreu, A. Morata, M. Skoumal, J. Rubio-Garcia, J. R. Morante, *RSC Adv.* **2013**, *3*, 12056–12059.
[6] C. Flox, M. Skoumal, J. Rubio-Garcia, T. Andreu, J. R. Morante, *Appl. Energy* **2013**, *109*, 344–351.
[7] M. Duduta, B. Ho, V. C. Wood, P. Limthongkul, V. E. Brunini, W. C. Carter, Y.-M. Chiang, *Adv. Energy Mater.* **2011**, *1*, 511–516.
[8] E. Ventosa, M. Skoumal, F. J. Vazquez, C. Flox, J. Albiol, J. R. Morante, *ChemSusChem*, **2015**, DOI: 10.1002/cssc.201500349.
[9] L. Madec, M. Youssry, M. Cerbelaud, P. Soudan, D. Guyomard, B. Lestriez, *J. Electrochem. Soc.* **2014**, *161*, A693–A699.
[10] S. Hamelet, D. Larcher, L. Dupont, J.-M. Tarascon, *J. Electrochem. Soc.* **2013**, *160*, A516–A520.
[11] T. Doherty, P. Limthongkul, A. Butros, M. Duduta, J. C. Cross (24 M Technologies, Inc.), US 2013/0337319 A1, **2013**.
[12] M. Youssry, L. Madec, P. Soudan, M. Cerbelaud, D. Guyomard, B. Lestriez, *Phys. Chem. Chem. Phys.* **2013**, *15*, 14476.
[13] S. Hamelet, T. Tzedakis, J.-B. Leriche, S. Sailler, D. Larcher, P.-L. Taberna, P. Simon, J.-M. Tarascon, *J. Electrochem. Soc.* **2012**, *159*, A1360–A1367.
[14] L. Madec, M. Youssry, M. Cerbelaud, P. Soudan, D. Guyomard, B. Lestriez, *ChemPlusChem* **2015**, *80*, 396–401.
[15] E. Ventosa, G. Zampardi, C. Flox, F. La Mantia, W. Schuhmann, J. R. Morante, *Chem. Commun.* **2015**, *51*, 14973.
[16] M. Gaberscek, J. Moskon, B. Erjavec, R. Dominko, J. Jamnik, *Electrochem. Solid-State Lett.* **2008**, *11*, A170–A174.
[17] E. Barsoukov, J. H. Kim, J. H. Kim, C. O. Yoon, H. Lee, *J. Electrochem. Soc.* **1998**, *145*, A2711–A2717.
[18] S. S. Zhang, K. Xu, T. R. Jow, *Electrochim. Acta* **2006**, *51*, 1636–1640.
[19] T. J. Petek, N. C. Hoyt, R. F. Savinell, J. S. Wainright, *J. Electrochem. Soc.* **2016**, *163*, A5001–A5009.
[20] L. Liu, L. Chen, X. Huang, X.-Q. Yang, W.-S. Yoon, H. S. Lee, J. McBreen, *J. Electrochem. Soc.* **2004**, *151*, A1344–A1351.
[21] K. Y. Chung, W.-S. Yoon, H. S. Lee, J. McBreen, X.-Q. Yang, S. H. Oh, W. H. Ryu, J. L. Lee, W. I. Cho, *J. Power Sources* **2006**, *163*, 185–190.
[22] Inorganic Crystal Structure Database, http://cds.dl.ac.uk.
[23] J. T. Dudley, D. P. Wilkinson, G. Thomas, R. LeVae, S. Woo, H. Blom, C. Horvath, M. W. Juzkow, B. Denis, P. Juric, P. Aghakian, J. R. Dahn, *J. Power Sources* **1991**, *35*, 59–82.
[24] J. R. Macdonald, W. R. Kenan, *Impedance Spectroscopy: Emphasizing Solid Materials and Systems*, Wiley-VCH, Weinheim, **1987**.
[25] J. T. S. Irvine, D. C. Sinclair, A. R. West, *Adv. Mater.* **1990**, *2*, 132.
[26] J. J. Biendicho, A. R. West, *Solid State Ionics* **2012**, *226*, 41–52.
[27] E. J. Abram, d. c. Sinclair, A. R. West, *J. Electroceram.* **2001**, *7*, 179–188.
[28] A. Yano, S. Aoyama, M. Shikano, H. Sakaebe, K. Tatsumi, Z. Ogumi, *J. Electrochem. Soc.* **2015**, *162*, A3137–A3144.
[29] P. Samarasingha, D.-H. Tran-Nguyen, M. Behm, A. Wijayasinghe, *Electrochim. Acta* **2008**, *53*, 7995–8000.
[30] J. Wolfenstine, U. Lee, J. L. Allen, *J. Power Sources* **2006**, *154*, 287–289.
[31] M. Youssry, L. Madec, P. Soudan, M. Cerbelaud, D. Guyomard, B. Lestriez, *J. Power Sources* **2015**, *274*, 424–431.
[32] K. B. Hatzell, M. Boota, Y. Gogotsi, *Chem. Soc. Rev.* **2015**, *44*, 8664–8687.
[33] Bio-logic internal report, **2013**, Application note #49.
[34] EC-Lab software V10.40, Bio-Logic-Science Instruments, **1997–2014**.
[35] ZView Version 3.2b, **1990–2010**, Scribner Associates, Inc.